 doi:10.20944/preprints201808.0066.v1

*Article*

# Synergistic use of radar Sentinel-1 and optical Sentinel-2 imagery for crop mapping: a case study for Belgium

**Kristof Van Tricht [1,*], Anne Gobin [1], Sven Gilliams [1] and Isabelle Piccard [1]**

[1] VITO Remote Sensing, Boeretang 200, 2400 Mol, Belgium; Kristof.vantricht@vito.be (K.V.T.); anne.gobin@vito.be (A.G.); sven.gilliams@vito.be (S.G.); Isabelle.piccard@vito.be (I.P.)

* Correspondence: Kristof.vantricht@vito.be; Tel.: +32 14 33 67 36

**Abstract:** A timely inventory of agricultural areas and crop types is an essential requirement for ensuring global food security. Satellite remote sensing has proven to be an increasingly more reliable tool to identify crop types. With the Copernicus program and its Sentinel satellites, a growing source of satellite remote sensing data is publicly available at no charge. Here we used joint Sentinel-1 radar and Sentinel-2 optical imagery to create a crop map for Belgium. To ensure homogenous radar and optical input across the country, Sentinel-1 12-day backscatter composites were created after incidence angle normalization, and Sentinel-2 NDVI images were smoothed to yield dekadal cloud-free composites. An optimized random forest classifier predicted the 8 crop types with a maximum accuracy of 82% and a kappa coefficient of 0.77. We found that a combination of radar and optical imagery always outperformed a classification based on single-sensor inputs, and that classification performance increased throughout the season until July, when differences between crop types are largest. Furthermore we showed that the concept of classification confidence derived from the random forest classifier provided insight in the reliability of the predicted class for each pixel, clearly showing that parcel borders have a lower classification confidence. We concluded that the synergistic use of radar and optical data for crop classification led to richer information increasing classification accuracies compared to optical-only classification. Further work should focus on object-level classification and crop monitoring to exploit the rich potential of combined radar and optical observations.

**Keywords:** Crop classification; SAR; Optical; time series; Sentinel-1; Sentinel-2; random forest; machine learning

## 1. Introduction

One of the requirements for ensuring food security is a timely inventory of agricultural areas and the proportion of different crop types on the fields [1]. Satellite remote sensing has proven to be an invaluable tool for accurate crop mapping in regions across the world [2–5].

The most conventional way of performing satellite-based crop classifications is the use of optical imagery. This has started with the Landsat missions [6–8]. Gradually the spatial, temporal, and spectral resolution has increased since, constantly improving the classification results [9–12].

In June 2015, Sentinel-2 was launched as part of the Copernicus Sentinel-2 mission [13]. This mission consists of a constellation of two identical satellites, Sentinel-2A and Sentinel-2B. The revisit frequency of one satellite is 10 days, resulting in a revisit frequency of 5 days for the constellation. Sentinel-2 carries a MultiSpectral Instrument (MSI) with 13 bands in the visible, near infrared and shortwave infrared part of the spectrum. These state-of-the-art specifications have been used in recent research on crop classification [14].

A major drawback of optical sensors remains clouds that cannot be penetrated by optical radiation. Clouds and cloud shadows therefore lead to gaps in optical imagery, and missing data in

 doi:10.20944/preprints201808.0066.v1

optical time series [15]. For classification and monitoring purposes, this drawback can significantly affect performance.

Possible strategies to overcome the disadvantages of clouds and shadows are multi-sensor combinations, especially strategies that exploit different parts of the electromagnetic spectrum [16]. Microwave radiation in the C-band, for example, has wavelengths well above the typical size of cloud particles, and can therefore penetrate clouds mostly unaltered [17]. Satellite sensors exploiting this part of the spectrum need to send out their own energy pulse and subsequently measure the reflected energy. A synthetic aperture radar (SAR) is such a system that uses the motion of the instrument to attain a satisfactory ground resolution [17].

Although the potential of SAR observations from space has been demonstrated extensively, their availability in the past was restricted to specific campaigns [18,19]. However, with the advent of the Sentinel-1 mission, the SAR era has changed to a higher pace, with almost global data availability at no charge and regular time intervals [20,21]. The revisit frequency is 6 days now that both the Sentinel-1A as well as the Sentinel-1B satellites are operational. Considering overlap and combining ascending and descending orbits, this leads to a Sentinel-1 observation every ~2 days in Europe.

Contrary to optical imagery that provides insights into biophysical processes of vegetation, SAR imagery reflects the structural components of vegetation and the underlying surface, resulting in a complementary data source that can be used for crop classification and monitoring purposes [16,22–27].

The aim of this study is to quantify the added value of using synergistic optical Sentinel-2 and SAR Sentinel-1 imagery for a case study of crop classification in Belgium, and to develop classification procedures for efficient processing at country scale. The following questions are addressed in this work:

- How can optical and radar data be processed efficiently across swaths to suit a crop classification scheme?
- How does classification accuracy at pixel-level depend on the input source (optical, radar, or a combination of both)?
- How does classification accuracy evolve during the growing season?
- What is the classification confidence and how can this be used for assessing classification accuracy?

We first describe the relevant data sources used and the pre-processing routines for interoperability of Sentinel-1 and Sentinel-2 imagery. Next, a hierarchical classification methodology is discussed in view of different classification schemes. Finally, the results are discussed in light of croptype differences across the growing season.

## 2. Materials and Methods

### *2.1 Data*

#### 2.1.1 Field data

The Integrated Administration and Control System (IACS) is the most important system for the management and control of payments to farmers made by the Member States in application of the European Common Agricultural Policy. The Land Parcel Information System (LPIS) is the spatial database that permits spatial and alphanumeric queries and data retrieval in function of the subsidy application and administrative cross-checks. In Belgium this is arranged at the regional level, resulting in two similar datasets for the Flemish and the Walloon regions. From these datasets, crop cover per agricultural parcel was extracted.

Belgium's utilized agricultural land use covers 1,341,487 ha, out of which 30% is grassland, 2% permanent crops and 68% arable land. In order of importance, the main arable crops are winter wheat, maize, winter barley, potatoes, sugar beet and rapeseed.

Preprints (www.preprints.org) | NOT PEER-REVIEWED | Posted: 3 August 2018 doi:10.20944/preprints201808.0066.v1

2.1.2 Sentinel-1 data

The Sentinel-1 data originated from the Level-1 Ground Range Detected (GRD) Interferometric Wide Swath (IW) product as ingested in Google Earth Engine (GEE) [28]. This GRD product consisted of Sentinel-1 radar observations projected onto a regular 10m grid. The data were preprocessed by GEE using the Sentinel-1 toolbox. Preprocessing included thermal noise removal, radiometric calibration and terrain correction. The primary features recorded by Sentinel-1 over Belgium were the VV and VH polarized backscatter values (in decibels, dB). Backscatter is strongly influenced by the orientation of the emitted radar beam. Due to the significantly different viewing orientation between the ascending and descending satellite overpasses, these were separated and considered as complementary observations. We applied a refined Lee filter [29] to reduce radar speckle in the images .

To reduce the effects of incidence angle variations on the backscatter values, we performed two procedures. First, all observations recorded under an incidence angle below 32° or above 42° were disregarded since these viewing geometries are too different from the mean incidence angle in our region of 37°. Next, a square cosine correction is applied, as outlined in [30]. All remaining backscatter values as observed under an incidence angle $\theta$ were rescaled to backscatter values that would be observed under a reference angle $\theta_{ref}$, based Eq. (1).

$$\sigma^0_{\theta_{ref}} = \frac{\sigma^0_\theta \cos^2(\theta_{ref})}{\cos^2(\theta)} \quad (1)$$

In this equation, $\sigma^0_\theta$ is the backscatter intensity under the observed incidence angle $\theta$, and $\sigma^0_{\theta_{ref}}$ the estimated backscatter intensity under a reference angle $\theta_{ref}$ of 37°. This simplified correction was based on Lambert's law of optics and included assumptions about the scattering mechanisms. Lambert's law states that the amount of diffuse light that is reflected from an ideal lambertian surface reflector is equal in all directions and proportional to the cosine of the incidence angle of the radiation source. The earth surface, however, is not a homogeneous ideal lambertian reflector. For our classification purpose, this incidence angle correction was sufficient, as it removed the highest dependencies of the backscatter magnitudes on the observed incidence angles.

Finally, we created 12-day backscatter composites from the combined Sentinel-1A and Sentinel-1B observations. Given the revisit frequency of 12 days for each satellite, at least two observations were recorded within this timeframe. Our analyses showed that after masking extreme incidence angles, between 2 and 5 observations were recorded for each location within the 12-day timeframe. For each pixel, all recorded backscatter values within the 12-day window were converted from their decibel values to the original values, then averaged, and converted back to the 12-day composite backscatter values in decibels. An RGB example of three processed 12-day composites is shown in Figure 1. The backscatter composites were projected to the Belgian EPSG:31370 grid with a spatial resolution of 10m.

This processing workflow was conducted on all available Sentinel-1 imagery between March 1st 2017 and August 16th 2017, resulting in a total of 60 ascending and descending, VV and VH 12-day composites, used as input features in the classification procedure.

Preprints (www.preprints.org) | NOT PEER-REVIEWED | Posted: 3 August 2018 doi:10.20944/preprints201808.0066.v1

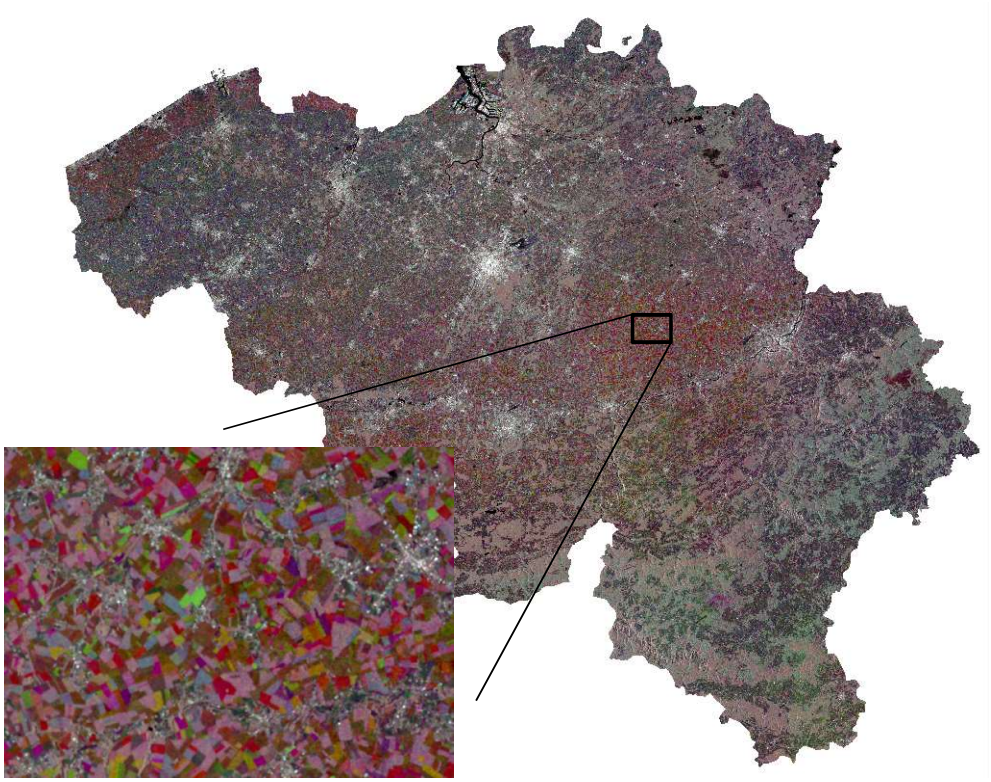

**Figure 1.** RGB image of 12-day Sentinel-1 VH backscatter composites. 1-13 March 2017 (red), 17-29 June 2017 (green), and 16-28 August 2017 (blue). Inset shows a detailed view of this RGB, demonstrating the rich information on agricultural land that is present in SAR backscatter observations.

2.1.3 Sentinel-2 data

The Sentinel-2 Level-1C data as retrieved from the Copernicus Open Access Hub, were first masked for clouds and cloud shadows by the Sen2Cor algorithm [31], and subsequently atmospherically corrected using the iCOR atmospheric correction scheme [32]. For poorly co-registered Sentinel-2 scenes (i.e. with a multi-temporal co-registration error > 0.5 pixels), an additional geometric correction was applied based on manually identified ground control points.

We used the NDVI value calculated from the red (B4) and near-infrared (B8) bands, both at a spatial resolution of 10m. These NDVI values served as input to the classification procedure. However, frequent and impartial cloud cover imposed a significant challenge for crop classification of a large area covering several image tiles. Cloud obstruction was removed using a pixel-wise weighted least squares smoothing of the NDVI values over time [33]. The smoothed NDVI images were produced at dekadal intervals between March 1st 2017 and August 31st 2017, resulting in a total of 18 input features for the classification. The final images were projected to the Belgian EPSG:31370 grid with a spatial resolution of 10m, similar to the Sentinel-1 images. An RGB example of three smoothed NDVI images is shown in Figure 2.

Preprints (www.preprints.org) | NOT PEER-REVIEWED | Posted: 3 August 2018 doi:10.20944/preprints201808.0066.v1

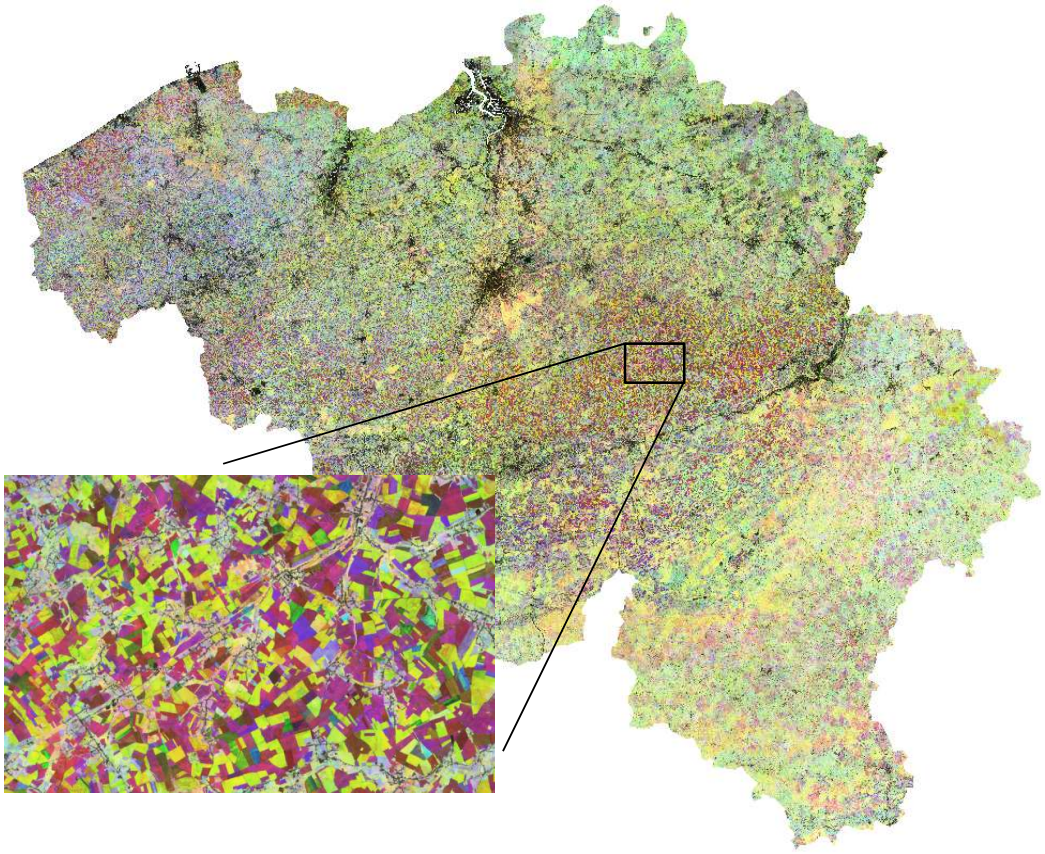

**Figure 2.** RGB image of smoothed NDVI. 1st dekad of March 2017 (red), last dekad of June 2017 (green), and last dekad of August 2017 (blue). Inset shows a detailed view of this RGB, demonstrating the differences in temporal NDVI composites across different agricultural parcels.

*2.2 Methodology*

2.2.1 Hierarchical random forest classification

The classification was performed by a Random Forest (RF) classifier, a decision tree learning algorithm that is part of the machine learning classifiers [34]. It is known for performing particularly well and efficiently on large input datasets with many different features [35].

A two-step hierarchical classification procedure was followed, in which a first step distinguished between a broad crop class, and forest, water and built-up classes. In a second step, the crop class was further classified into the different crop types including grassland. This hierarchical procedure is schematically outlined in Figure 3.

The optimal random forest parameters were determined using a grid-search approach [35]. These parameters included the number of trees, the impurity criterion, the minimum amount of samples required to split a node, the minimum amount of samples required to be at a leaf node and the maximum number of features to consider when looking for the best split. Classification of a sample resulted from the majority voting of class predictions across the trees in the forest.

Preprints (www.preprints.org) | NOT PEER-REVIEWED | Posted: 3 August 2018 doi:10.20944/preprints201808.0066.v1

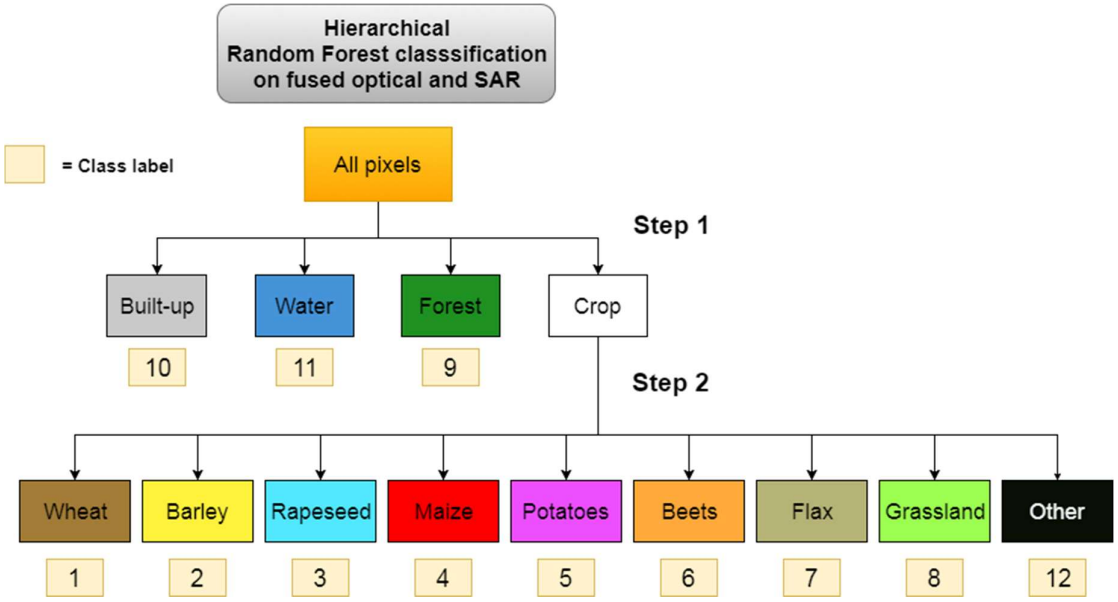


**Figure 3.** Schematic overview of the two-step hierarchical classification procedure.

2.2.2 Calibration and validation data

The classification procedure was trained based on the Flemish LPIS dataset. To ensure independent calibration and validation sets, the available parcels in the ground truth database were randomly subdivided in a 10% calibration set and a 90% validation set. The calibration parcels were subsequently subset on parcels above 2.5 ha which were expected to yield purer spectral signatures compared to the smaller fields. However, this area threshold was not applied to the validation set of parcels, which enabled the accuracy of classification on all parcel sizes. For a similar reason, the remaining calibration parcels were buffered 30m inward to avoid field border effects that could contaminate the spectral signatures during training. This buffer was not applied on the validation set. Finally, both the remaining calibration and validation parcels were rasterized to the 10m input imagery grid. Due to the different field sizes, the initial proportion of calibration and validation parcels was different from the proportion in pixels (Table 1).

**Table 1.** Total number of calibration and validation parcels and pixels per class

| Class | Calibration parcels | Validation parcels | Calibration pixels | Validation pixels |
|---|---|---|---|---|
| Wheat | 850 | 7653 | 171865 | 5700538 |
| Barley | 177 | 1591 | 31194 | 1333242 |
| Rapeseed | 9 | 78 | 1519 | 50163 |
| Maize | 1896 | 17065 | 293878 | 15614299 |
| Potatoes | 614 | 5523 | 121882 | 3867266 |
| Beets | 354 | 3182 | 73060 | 1913307 |
| Flax | 65 | 580 | 15118 | 366584 |
| Grassland | 2617 | 23557 | 322422 | 21200413 |
| Forest | 84 | 21 | 180783 | 282571 |
| Built-up | 39 | 10 | 20895 | 28180 |
| Water | 54 | 14 | 35628 | 54996 |
| Other | 825 | 8236 | 158273 | 6103789 |
| **Total** | **7,584** | **67,510** | **1,426,517** | **56,515,348** |

Preprints (www.preprints.org) | NOT PEER-REVIEWED | Posted: 3 August 2018 doi:10.20944/preprints201808.0066.v1

2.2.3 Classification schemes

A major aim of this study was to quantify the contribution of individual and combined optical and SAR imagery to the classification accuracy. In addition, an objective insight into the evolution of the classification accuracy during the growing season would yield useful information with regard to the expected accuracy of a classification at a certain period in the growing season.

We specified 18 classification schemes. In the first six schemes, only Sentinel-1 SAR imagery was used with increasing frequency from only one month (March 2017) to the entire period (March – August 2017). In the next schemes, a similar approach was followed for Sentinel-2 NDVI images, while the last six schemes followed the same procedure for combined Sentinel-1 and Sentinel-2 imagery.

For each classification scheme, the overall accuracy (OA) is calculated as the classifier performance estimator. The OA is defined as:

$$OA = \frac{\sum correct\ predictions}{total\ number\ of\ predictions} \quad (2)$$

where predictions were calculated for all available validation samples and the predicted labels were compared to the true labels.

2.2.4 Classification confidence

In addition to the classification, the random forest classifier was used to provide insight into the expected classification confidence. The confidence was estimated from the predicted class probabilities [36], which reflect the convergence of the classifier for each sample. In our setup of the random forest, the predicted class probabilities of an input sample were computed as the mean predicted class probabilities of the trees in the forest, which naturally sum to unity. We defined the classification confidence for a certain sample as the class probability of the winning class. A high confidence reflects strong agreement across the different trees and a more reliable classification, while a low confidence reflects disagreement between the trees and likely a less reliable classification. In addition to a general accuracy assessment of the produced classification, this analysis allows a much more specific assessment of classification confidence on a sample or pixel level.

## 3. Results

Table 2 demonstrates the evolution of the OA for the different classification schemes. As expected, OA increased gradually with the amount of input images during the season. This was explained by the increased discriminating power of a classifier when more information was added and differences between the different crop types became more apparent [22].

The classification result using Sentinel-1 in March was significantly better than using Sentinel-2 in March (47% vs 39%), while the overall accuracy of optical-only classification across the whole season performed slightly better than SAR-only classification across the season (78% vs 76%). This suggests that different crop types had comparable optical spectral features in their early stages, while their structure, reflected by the backscatter signatures, appeared more different. However, this was only the case for crop types such as winter cereals which were already on the field during this period. For crop types such as maize and potato that were planted in April-May, optical and radar signatures in March reflected the winter cover crop and management practices, and a direct link between these signatures and the classification performance for the main crop was not straightforward.

In each month, the cumulative number of images used demonstrated that a combination of Sentinel-1 and Sentinel-2 performed better than using a single sensor (Table 2). By the end of July, a maximum accuracy of 82% was reached, which could not be improved by adding the August imagery.

**Table 2.** Overall Accuracy (OA) of the different classification schemes.

 doi:10.20944/preprints201808.0066.v1

| Sentinel-2 | | | | | | Sentinel-1 | | | | | | |
|---|---|---|---|---|---|---|---|---|---|---|---|---|
| **Mar** | **Apr** | **May** | **Jun** | **Jul** | **Aug** | **Mar** | **Apr** | **May** | **Jun** | **Jul** | **Aug** | **OA** |
| | | | | | | X | | | | | | **0.47** |
| | | | | | | X | X | | | | | **0.62** |
| | | | | | | X | X | X | | | | **0.70** |
| | | | | | | X | X | X | X | | | **0.74** |
| | | | | | | X | X | X | X | X | | **0.75** |
| | | | | | | X | X | X | X | X | X | **0.76** |
| X | | | | | | | | | | | | **0.39** |
| X | X | | | | | | | | | | | **0.54** |
| X | X | X | | | | | | | | | | **0.66** |
| X | X | X | X | | | | | | | | | **0.72** |
| X | X | X | X | X | | | | | | | | **0.76** |
| X | X | X | X | X | X | | | | | | | **0.78** |
| X | | | | | | X | | | | | | **0.53** |
| X | X | | | | | X | X | | | | | **0.66** |
| X | X | X | | | | X | X | X | | | | **0.75** |
| X | X | X | X | | | X | X | X | X | | | **0.79** |
| X | X | X | X | X | | X | X | X | X | X | | **0.82** |
| X | X | X | X | X | X | X | X | X | X | X | X | **0.82** |

Figure 4 shows the final classification result by the end of August 2017, based on the combination of Sentinel-1 and -2 inputs. The detailed inset demonstrates a surprisingly smooth result of the classified parcels in a highly diverse arable landscape, given that no prior segmentation technique, nor a post-classification filtering method was applied.

The results (Table 2) were also apparent in Figure 5**Error! Reference source not found.**, where for the center field which is part of the validation dataset, certain within-field zones were wrongly classified as beet in the early mapping stage (taken here as June 2017), while these same zones were correctly identified as potato by the end of August.

Preprints (www.preprints.org) | NOT PEER-REVIEWED | Posted: 3 August 2018 doi:10.20944/preprints201808.0066.v1

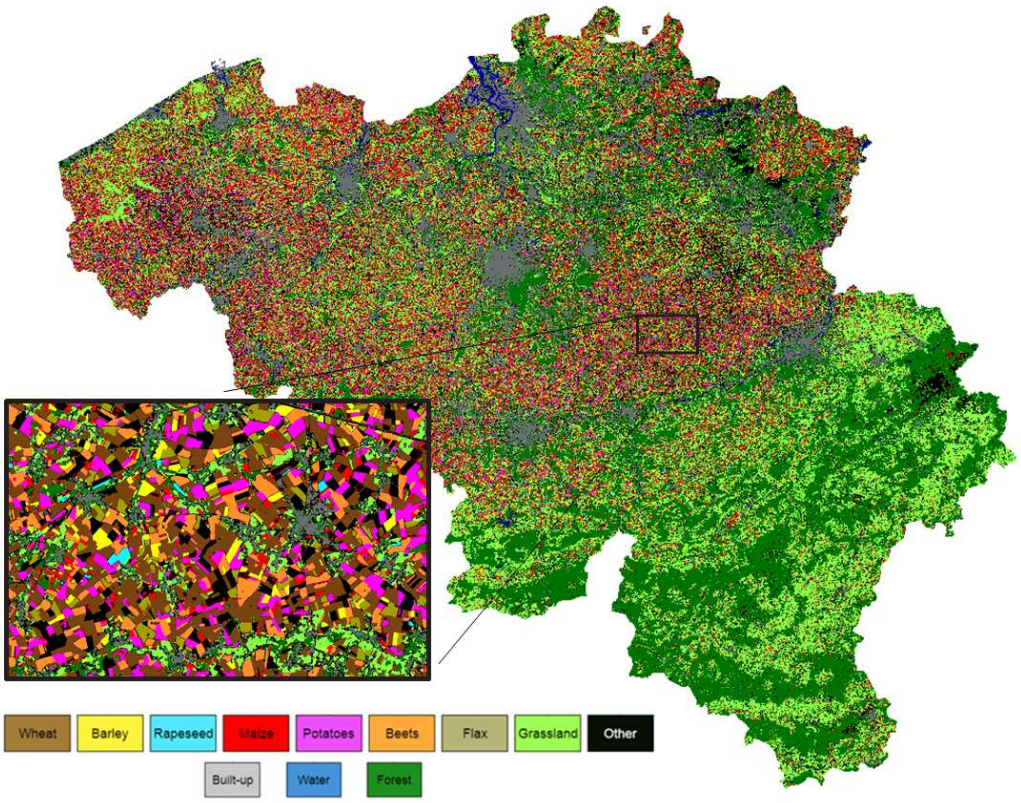


**Figure 4.** Final classification result by the end of August 2017 based on Sentinel-1 and -2 inputs. Inset shows a detailed view on the classification results in a highly diverse arable landscape.

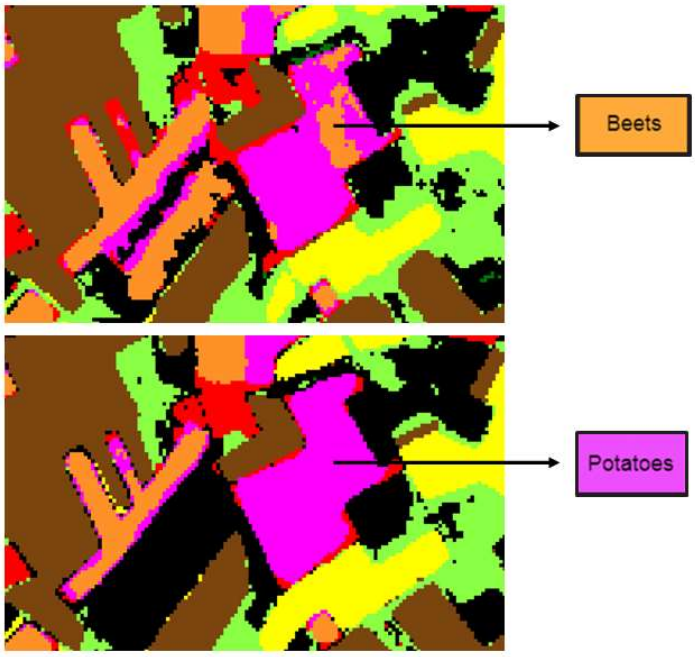


**Figure 5.** The combined Sentinel-1 and -2 classification result of June (upper) shows more within-field variability than the classification result of August (lower). In this particular example, the zones in the center field that were wrongly classified as beet in June, were correctly classified as potato in August.

Preprints (www.preprints.org) | NOT PEER-REVIEWED | Posted: 3 August 2018 doi:10.20944/preprints201808.0066.v1

This is further illustrated with the confusion matrix (Table 3 and Table 4). Early mapping in June led to an OA of 75% (corresponding to a kappa coefficient of 0.66), with typical confusion occurring between winter cereals, maize and grassland on the one hand, and potato and beet on the other hand. Confusion between the "other crop" class that contained the less frequent crop types and the larger crop classes was also considerable. By the end of August, OA has increased to 82.5% (corresponding to a kappa coefficient of 0.77), and all confusion values have decreased considerably. The "other crop" class remained challenging, due the high intra-class variability for this mix of different crop types. While training was limited to the Flanders region, classification was applied to the whole of Belgium. Since crop types and management practices can differ considerably between regions in Belgium, an independent validation was carried out using the Walloon LPIS dataset which was not used during training, resulting in an OA of 82% for early mapping in June and 86% for mapping in August. These values were slightly higher than in Flanders, mostly because the fields were larger and more homogeneous in the Walloon region.

The classification confidence map is shown in Figure 6 and it is clear from the detailed subset that the confidence was lowest near the edges of the parcels. Border pixels were typically showing contaminated spectral features, due to a mixture with surrounding land cover signals. This is further illustrated in Figure 7, where the borders near the center parcel were classified differently, but the associated confidence map shows that these border results had a high uncertainty. The true crop of this parcel was sugar beet, as correctly identified in the middle of the parcel with high confidence.

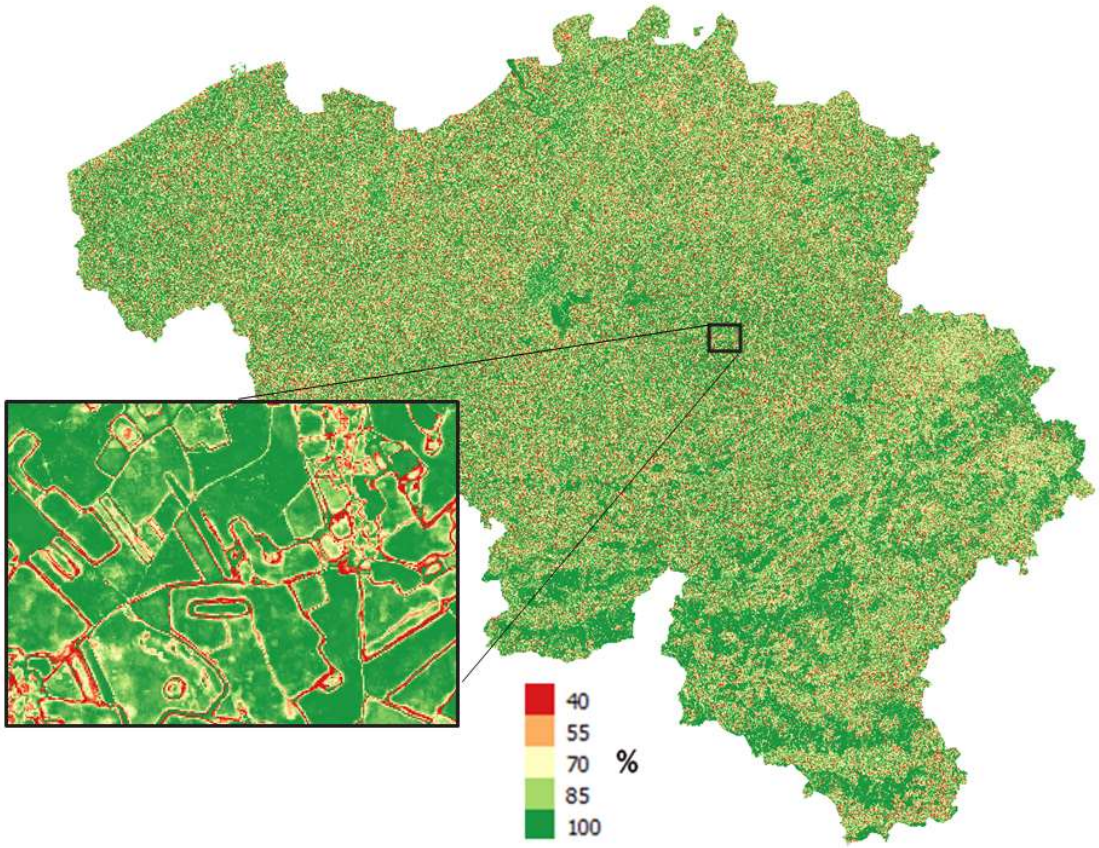


**Figure 6.** Classification confidence, defined as the random forest predicted class probability of the majority class for each pixel. Inset shows that the confidence was typically lower at the field borders, which can be explained by spectral contamination of pixels near field edges.

 doi:10.20944/preprints201808.0066.v1

**Table 3.** Confusion matrix for early mapping in June 2017 using Sentinel-1 and -2 inputs.

| | Wheat | Barley | Rapeseed | Maize | Potatoes | Beets | Flax | Grassland | Forest | Built-up | Water | Other crop | Total true |
|---|---|---|---|---|---|---|---|---|---|---|---|---|---|
| **Wheat** | 7.6 | 0.0 | 0.0 | 0.9 | 0.1 | 0.0 | 0.0 | 1.1 | 0.0 | 0.0 | 0.0 | 0.4 | **10.1** |
| **Barley** | 0.0 | 1.5 | 0.0 | 0.2 | 0.0 | 0.0 | 0.0 | 0.4 | 0.0 | 0.0 | 0.0 | 0.1 | **2.4** |
| **Rapeseed** | 0.0 | 0.0 | 0.1 | 0.0 | 0.0 | 0.0 | 0.0 | 0.0 | 0.0 | 0.0 | 0.0 | 0.0 | **0.1** |
| **Maize** | 0.1 | 0.0 | 0.0 | 22.2 | 0.3 | 0.0 | 0.0 | 2.4 | 0.3 | 0.1 | 0.0 | 2.1 | **27.6** |
| **Potato** | 0.0 | 0.0 | 0.0 | 1.2 | 4.9 | 0.2 | 0.0 | 0.1 | 0.0 | 0.0 | 0.0 | 0.4 | **6.8** |
| **Beet** | 0.0 | 0.0 | 0.0 | 0.5 | 0.6 | 2.0 | 0.0 | 0.1 | 0.0 | 0.0 | 0.0 | 0.2 | **3.4** |
| **Flax** | 0.0 | 0.0 | 0.0 | 0.1 | 0.0 | 0.0 | 0.4 | 0.1 | 0.0 | 0.0 | 0.0 | 0.1 | **0.6** |
| **Grassland** | 0.1 | 0.0 | 0.0 | 1.3 | 0.1 | 0.0 | 0.0 | 31.2 | 1.3 | 0.3 | 0.0 | 3.2 | **37.5** |
| **Forest** | 0.0 | 0.0 | 0.0 | 0.0 | 0.0 | 0.0 | 0.0 | 0.0 | 0.5 | 0.0 | 0.0 | 0.0 | **0.5** |
| **Built-up** | 0.0 | 0.0 | 0.0 | 0.0 | 0.0 | 0.0 | 0.0 | 0.0 | 0.0 | 0.0 | 0.0 | 0.0 | **0.0** |
| **Water** | 0.0 | 0.0 | 0.0 | 0.0 | 0.0 | 0.0 | 0.0 | 0.0 | 0.0 | 0.0 | 0.1 | 0.0 | **0.1** |
| **Other crop** | 0.2 | 0.0 | 0.0 | 1.9 | 0.4 | 0.1 | 0.0 | 3.3 | 0.3 | 0.1 | 0.0 | 4.4 | **10.8** |
| **Total est.** | **8.1** | **1.6** | **0.1** | **28.2** | **6.4** | **2.4** | **0.4** | **38.7** | **2.4** | **0.6** | **0.1** | **11.0** | **OA = 75%** |

**Table 4.** Confusion matrix for final mapping in August 2017 using Sentinel-1 and -2 inputs.

| | Wheat | Barley | Rapeseed | Maize | Potatoes | Beets | Flax | Grassland | Forest | Built-up | Water | Other crop | Total true |
|---|---|---|---|---|---|---|---|---|---|---|---|---|---|
| **Wheat** | 8.6 | 0.1 | 0.0 | 0.1 | 0.0 | 0.0 | 0.0 | 0.5 | 0.0 | 0.0 | 0.0 | 0.7 | **10.1** |
| **Barley** | 0.0 | 1.9 | 0.0 | 0.0 | 0.0 | 0.0 | 0.0 | 0.2 | 0.0 | 0.0 | 0.0 | 0.2 | **2.4** |
| **Rapeseed** | 0.0 | 0.0 | 0.1 | 0.0 | 0.0 | 0.0 | 0.0 | 0.0 | 0.0 | 0.0 | 0.0 | 0.0 | **0.1** |
| **Maize** | 0.0 | 0.0 | 0.0 | 24.6 | 0.4 | 0.0 | 0.0 | 0.9 | 0.3 | 0.1 | 0.0 | 1.3 | **27.6** |
| **Potato** | 0.0 | 0.0 | 0.0 | 1.1 | 5.2 | 0.1 | 0.0 | 0.0 | 0.0 | 0.0 | 0.0 | 0.4 | **6.8** |
| **Beet** | 0.0 | 0.0 | 0.0 | 0.3 | 0.5 | 2.4 | 0.0 | 0.0 | 0.0 | 0.0 | 0.0 | 0.1 | **3.4** |
| **Flax** | 0.0 | 0.0 | 0.0 | 0.0 | 0.0 | 0.0 | 0.5 | 0.0 | 0.0 | 0.0 | 0.0 | 0.1 | **0.7** |
| **Grassland** | 0.1 | 0.0 | 0.0 | 0.8 | 0.0 | 0.0 | 0.0 | 32.2 | 0.8 | 0.3 | 0.0 | 3.2 | **37.5** |
| **Forest** | 0.0 | 0.0 | 0.0 | 0.0 | 0.0 | 0.0 | 0.0 | 0.0 | 0.5 | 0.0 | 0.0 | 0.0 | **0.5** |
| **Built-up** | 0.0 | 0.0 | 0.0 | 0.0 | 0.0 | 0.0 | 0.0 | 0.0 | 0.0 | 0.0 | 0.0 | 0.0 | **0.1** |
| **Water** | 0.0 | 0.0 | 0.0 | 0.0 | 0.0 | 0.0 | 0.0 | 0.0 | 0.0 | 0.0 | 0.1 | 0.0 | **0.1** |
| **Other crop** | 0.2 | 0.0 | 0.0 | 0.9 | 0.2 | 0.0 | 0.0 | 2.6 | 0.2 | 0.1 | 0.0 | 6.4 | **10.8** |
| **Total est.** | **9.0** | **2.0** | **0.1** | **27.9** | **6.4** | **2.6** | **0.5** | **36.5** | **1.9** | **0.7** | **0.1** | **12.4** | **OA = 82.5%** |

Preprints (www.preprints.org) | NOT PEER-REVIEWED | Posted: 3 August 2018 doi:10.20944/preprints201808.0066.v1

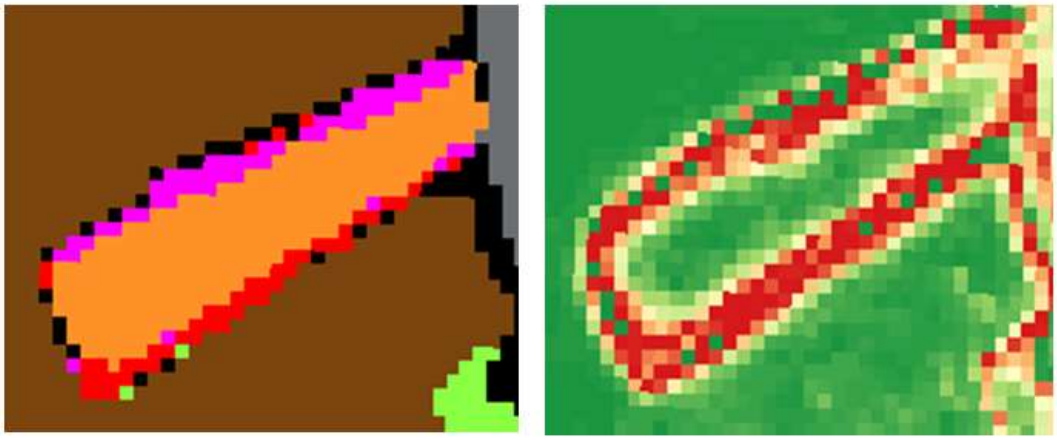

**Figure 7.** Detail of classification result (left) and classification confidence (right), demonstrating that the classification confidence near the field borders is significantly lower. In this specific example, the crop class is sugar beet, as correctly classified in the center of the field.

## 4. Discussion

Crop classification requires uniform inputs across the whole region. For Sentinel-1, this was accomplished by creating 12-day backscatter composites in which special care was taken to reduce incidence angle effects on the results. For Sentinel-2, this was realized by smoothing all cloud-free NDVI observations at pixel-level and creating dekadal cloud-free NDVI mosaics. These time series inputs were used in a hierarchical random forest classification to yield a crop map for the whole of Belgium.

The overall accuracy clearly increased along the growing season. However, typical summer crops such as potato, maize and sugar beet well emerged only by the end of May. Winter cereals, in turn, were already well developed by then. This led to classification accuracies of particular crop types deviating considerably from the OA. For example, winter cereals were mapped against the other crops by the end of May with a user's accuracy of 96% and a producer's accuracy of 71%, while potato was mapped against the other crops with a user's accuracy of 86% and a producer's accuracy of only 40%. This demonstrates how the accuracy within the growing season depends strongly on the evolution of the crop's phenological stages. These insights agree with previous research showing that using optical time series which include phenological differences in classification tasks has a positive impact on the performance [12].

The increasing OA during the season leads to a tradeoff: where the quality of the classification results improved with time, the timeliness of the results decreased. Our analysis provided insight into this tradeoff and may help choose the appropriate time in the growing season for a specific application where crop classification is needed.

The classification confidence was shown to provide helpful insights at the pixel-level with regard to the quality of classification. We investigated to which degree this confidence could be used to assess the classification performance, by quantifying the mean classification accuracy in function of the classification confidence (Figure 8). The strongly positive correlation between both indicated that the produced confidence estimates could be used to assess the expected classification accuracy. However, this confidence is not equal to a statistical probability and should not be used as such.

Preprints (www.preprints.org) | NOT PEER-REVIEWED | Posted: 3 August 2018 doi:10.20944/preprints201808.0066.v1

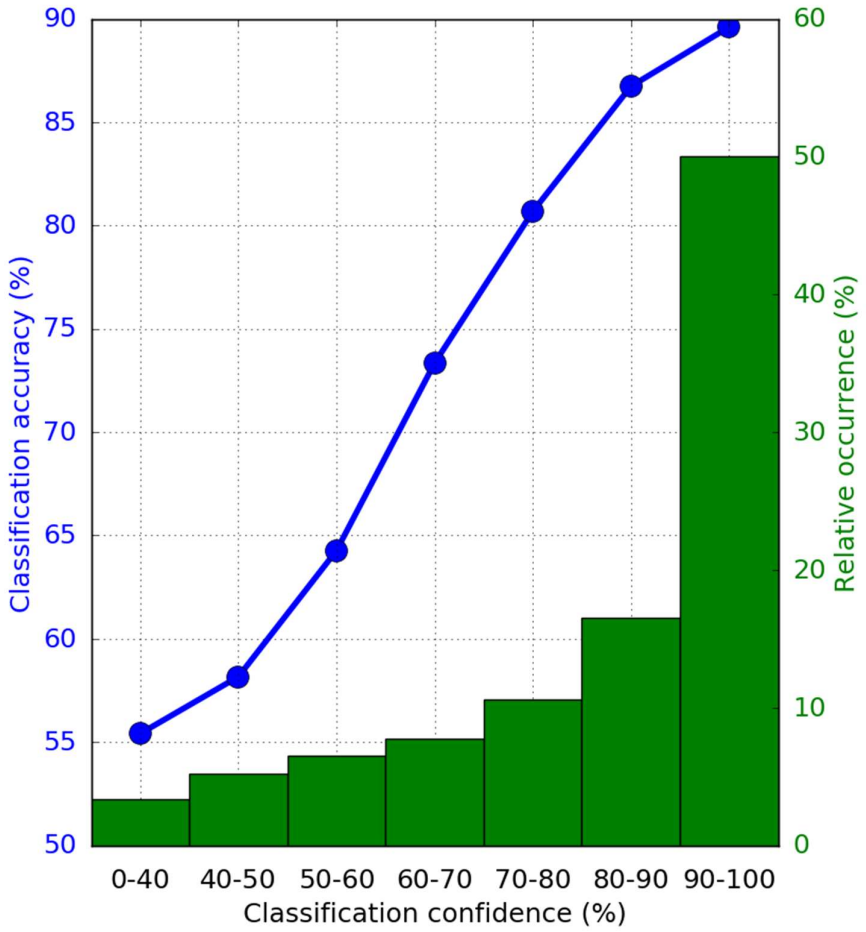


**Figure 8.** Mean classification accuracy in function of classification confidence, as well as the relative occurrence of each confidence level. This analysis clearly demonstrates the strong correlation between accuracy and confidence, meaning that the confidence level can be qualitatively used to assess the expected accuracy of the classification in a specific region.

NDVI is not a full descriptor of Sentinel-2 optical imagery, although it has been used successfully in the past [37]. It is therefore often beneficial to use more bands, especially when exclusively using optical imagery [38]. However, it was not the aim of this work to maximize classification accuracy solely based on optical images. When using optical imagery in combination with radar imagery, a stack of NDVI images throughout the growing season yields sufficient optical descriptors to classify crops, although the addition of other optical metrics could be subject to future research.

Our results clearly showed the advantage of using complementary Sentinel-1 SAR observations that give insight into the plant structural components [39]. The better classification performance we found is largely in agreement with other studies [16,22–24,27,40–44].

Further steps could include working on feature instead of pixel level, where combined Sentinel-1 and Sentinel-2 observations could serve as input to an automatic parcel detection tool. Classification can subsequently be performed at the parcel-level with the strong advantage that spectral signatures can be averaged for a field, significantly increasing the signal-to-noise ratio [45]. This is especially beneficial for analyzing radar signatures, where reduced radar speckle at the parcel level will decrease intra-class variability and increase inter-class variability, thereby improving classification accuracies.

 doi:10.20944/preprints201808.0066.v1

## 5. Conclusions

Growing food demands require timely estimates of crop acreages at large scale. Identification of different crop types forms the basis for such tasks. State-of-the-art earth observation technologies allow such identification from space. With the unprecedented potential of sensor synergies in the Copernicus program, multi-sensor classification procedures that go beyond traditional optical-only procedures can now be developed operationally.

Previous research clearly demonstrated the complementary nature of optical and radar signals to improve classification accuracies, in addition to alleviating cloud obstruction and therefore challenging optical-only monitoring of vegetation.

We created 12-day Sentinel-1 backscatter composites and decadal sSentinel-2 smoothed NDVI composites over Belgium to develop a multi-sensor crop mapping approach tested on the 2017 growing season. Based on an optimized random forest classifier, we predicted 8 different crop types with a maximum accuracy of 82% and a kappa coefficient of 0.77. The combination of radar and optical always outperformed a single-sensor classification procedure, with a clearly increasing accuracy throughout the growing season up till July when the maximum mapping accuracy was reached. The concept of classification confidence was shown to provide additional information going beyond a hard classification result, indicating regions where confidence is lower such as near parcel boundaries.

These results urge the need for multi-sensor crop classification and monitoring efforts, to fully exploit the rich potential of existing and future complementary satellite sensors.

**Author Contributions:** Conceptualization, Kristof Van Tricht; Funding acquisition, Isabelle Piccard; Methodology, Kristof Van Tricht, Anne Gobin and Isabelle Piccard; Supervision, Sven Gilliams and Isabelle Piccard; Writing – original draft, Kristof Van Tricht; Writing – review & editing, Anne Gobin, Sven Gilliams and Isabelle Piccard.

**Funding:** This research was funded as part of the BELCAM project by the Belgian Science Policy Office (BELSPO) under contract SR/00/300 of the STEREO II program.

**Acknowledgments:** We would like to thank the BELCAM team for their constructive remarks.

**Conflicts of Interest:** The authors declare no conflict of interest. The funders had no role in the design of the study; in the collection, analyses, or interpretation of data; in the writing of the manuscript, and in the decision to publish the results.

## References


1. Thenkabail, P. S. Global Croplands and their Importance for Water and Food Security in the Twenty-first Century: Towards an Ever Green Revolution that Combines a Second Green Revolution with a Blue Revolution. *Remote Sens.* **2010**, *2*, 2305–2312, doi:10.3390/rs2092305.

2. Wardlow, B. D.; Egbert, S. L. Large-area crop mapping using time-series MODIS 250 m NDVI data: An assessment for the U.S. Central Great Plains. *Remote Sens. Environ.* **2008**, *112*, 1096–1116, doi:10.1016/j.rse.2007.07.019.

3. Arvor, D.; Jonathan, M.; Meirelles, M. S. P.; Dubreuil, V.; Durieux, L. Classification of MODIS EVI time series for crop mapping in the state of Mato Grosso, Brazil. *Int. J. Remote Sens.* **2011**, *32*, 7847–7871, doi:10.1080/01431161.2010.531783.

4. Kussul, N.; Skakun, S.; Shelestov, A.; Lavreniuk, M.; Yailymov, B.; Kussul, O. Regional scale crop mapping using multi-temporal satellite imagery. *ISPRS - Int. Arch. Photogramm. Remote Sens. Spat. Inf. Sci.* **2015**, *XL-7/W3*, 45–52, doi:10.5194/isprsarchives-XL-7-W3-45-2015.

5. Panigrahy, S.; Sharma, S. A. Mapping of crop rotation using multidate Indian Remote Sensing Satellite digital data. *ISPRS J. Photogramm. Remote Sens.* **1997**, *52*, 85–91, doi:10.1016/S0924-2716(97)83003-1.

6. JANSSEN, L. L. F.; MIDDELKOOP, H. Knowledge-based crop classification of a Landsat Thematic Mapper image. *Int. J. Remote Sens.* **1992**, *13*, 2827–2837, doi:10.1080/01431169208904084.

7. Bauer, M. E.; Cipra, J. E.; Anuta, P. E.; Etheridge, J. B. Identification and area estimation of agricultural crops by computer classification of LANDSAT MSS data. *Remote Sens. Environ.* **1979**, *8*, 77–92, doi:10.1016/0034-4257(79)90025-7.

8. BATISTA, G. T.; HIXSON, M. M.; BAUER, M. E. LANDSAT MSS crop classification performance as a function of scene characteristics. *Int. J. Remote Sens.* **1985**, *6*, 1521–1533, doi:10.1080/01431168508948298.

9. Tatsumi, K.; Yamashiki, Y.; Canales Torres, M. A.; Taipe, C. L. R. Crop classification of upland fields using Random forest of time-series Landsat 7 ETM+ data. *Comput. Electron. Agric.* **2015**, *115*, 171–179, doi:10.1016/j.compag.2015.05.001.

10. Li, Q.; Wang, C.; Zhang, B.; Lu, L. Object-Based Crop Classification with Landsat-MODIS Enhanced Time-Series Data. *Remote Sens.* **2015**, *7*, 16091–16107, doi:10.3390/rs71215820.

11. Jia, K.; Wei, X.; Gu, X.; Yao, Y.; Xie, X.; Li, B. Land cover classification using Landsat 8 Operational Land Imager data in Beijing, China. *Geocarto Int.* **2014**, *29*, 941–951, doi:10.1080/10106049.2014.894586.

12. Durgun, Y.; Gobin, A.; Van De Kerchove, R.; Tychon, B. Crop Area Mapping Using 100-m Proba-V Time Series. *Remote Sens.* **2016**, *8*, 585, doi:10.3390/rs8070585.

13. Drusch, M.; Del Bello, U.; Carlier, S.; Colin, O.; Fernandez, V.; Gascon, F.; Hoersch, B.; Isola, C.; Laberinti, P.; Martimort, P.; Meygret, A.; Spoto, F.; Sy, O.; Marchese, F.; Bargellini, P. Sentinel-2: ESA's Optical High-Resolution Mission for GMES Operational Services. *Remote Sens. Environ.* **2012**, *120*, 25–36,

doi:10.1016/j.rse.2011.11.026.

14. Immitzer, M.; Vuolo, F.; Atzberger, C. First Experience with Sentinel-2 Data for Crop and Tree Species Classifications in Central Europe. *Remote Sens.* **2016**, *8*, 166, doi:10.3390/rs8030166.

15. Baret, F.; Weiss, M.; Lacaze, R.; Camacho, F.; Makhmara, H.; Pacholcyzk, P.; Smets, B. GEOV1: LAI and FAPAR essential climate variables and FCOVER global time series capitalizing over existing products. Part1: Principles of development and production. *Remote Sens. Environ.* **2013**, *137*, 299–309, doi:10.1016/j.rse.2012.12.027.

16. Joshi, N.; Baumann, M.; Ehammer, A.; Fensholt, R.; Grogan, K.; Hostert, P.; Jepsen, M. R.; Kuemmerle, T.; Meyfroidt, P.; Mitchard, E. T. A.; Reiche, J.; Ryan, C. M.; Waske, B. A review of the application of optical and radar remote sensing data fusion to land use mapping and monitoring. *Remote Sens.* **2016**, *8*, 1–23, doi:10.3390/rs8010070.

17. Campbell, J. B.; Wynne, R. H. *Introduction to Remote Sensing, Fifth Edition*; The Guilford Press; 5th edition, 2011; ISBN 160918176X.

18. Kasischke, E. S.; Melack, J. M.; Craig Dobson, M. The use of imaging radars for ecological applications—A review. *Remote Sens. Environ.* **1997**, *59*, 141–156, doi:10.1016/S0034-4257(96)00148-4.

19. McNairn, H.; Brisco, B. The application of C-band polarimetric SAR for agriculture: a review. *Can. J. Remote Sens.* **2004**, *30*, 525–542, doi:10.5589/m03-069.

20. Torres, R.; Snoeij, P.; Geudtner, D.; Bibby, D.; Davidson, M.; Attema, E.; Potin, P.; Rommen, B.; Floury, N.; Brown, M.; Traver, I. N.; Deghaye, P.; Duesmann, B.; Rosich, B.; Miranda, N.; Bruno, C.; L'Abbate, M.; Croci, R.; Pietropaolo, A.; Huchler, M.; Rostan, F. GMES Sentinel-1 mission. *Remote Sens. Environ.* **2012**, *120*, 9–24, doi:10.1016/j.rse.2011.05.028.

21. Malenovský, Z.; Rott, H.; Cihlar, J.; Schaepman, M. Sentinels for science: Potential of Sentinel-1,-2, and-3 missions for scientific observations of ocean, cryosphere, and land. *Remote Sens.* **2012**.

22. McNairn, H.; Champagne, C.; Shang, J.; Holmstrom, D.; Reichert, G. Integration of optical and Synthetic Aperture Radar (SAR) imagery for delivering operational annual crop inventories. *ISPRS J. Photogramm. Remote Sens.* **2009**, *64*, 434–449, doi:10.1016/j.isprsjprs.2008.07.006.

23. Ferrant, S.; Selles, A.; Le Page, M.; Herrault, P. A.; Pelletier, C.; Al-Bitar, A.; Mermoz, S.; Gascoin, S.; Bouvet, A.; Saqalli, M.; Dewandel, B.; Caballero, Y.; Ahmed, S.; Maréchal, J.-C.; Kerr, Y. Detection of Irrigated Crops from Sentinel-1 and Sentinel-2 Data to Estimate Seasonal Groundwater Use in South India. *Remote Sens.* **2017**, *In Press*, doi:10.3390/rs9111119.

24. Zhou, T.; Pan, J.; Zhang, P.; Wei, S.; Han, T. Mapping Winter Wheat with Multi-Temporal SAR and Optical Images in an Urban Agricultural Region. **2017**, 1–16, doi:10.3390/s17061210.

25. Lehmann, E. A.; Caccetta, P.; Lowell, K.; Mitchell, A.; Zhou, Z. S.; Held, A.; Milne, T.; Tapley, I. SAR and optical remote sensing: Assessment of complementarity and interoperability in the context of a large-scale operational forest monitoring system. *Remote Sens. Environ.* **2015**, *156*, 335–348,

doi:10.1016/j.rse.2014.09.034.

26. Rüetschi, M.; Schaepman, M.; Small, D. Using Multitemporal Sentinel-1 C-band Backscatter to Monitor Phenology and Classify Deciduous and Coniferous Forests in Northern Switzerland. *Remote Sens.* **2017**, *10*, 55, doi:10.3390/rs10010055.

27. Soria-Ruiz, J.; Fernandez-Ordoñez, Y.; Woodhouse, I. H. Land-cover classification using radar and optical images: a case study in Central Mexico. *Int. J. Remote Sens.* **2010**, *31*, 3291–3305, doi:10.1080/01431160903160777.

28. Gorelick, N.; Hancher, M.; Dixon, M.; Ilyushchenko, S.; Thau, D.; Moore, R. Google Earth Engine: Planetary-scale geospatial analysis for everyone. *Remote Sens. Environ.* **2017**, *202*, 18–27, doi:10.1016/j.rse.2017.06.031.

29. Lee, J.-S. Refined filtering of image noise using local statistics. *Comput. Graph. Image Process.* **1981**, *15*, 380–389, doi:10.1016/S0146-664X(81)80018-4.

30. Topouzelis, K.; Singha, S.; Kitsiou, D. Incidence angle normalization of Wide Swath SAR data for oceanographic applications. *Open Geosci.* **2016**, *8*, doi:10.1515/geo-2016-0029.

31. Main-Knorn, M.; Pflug, B.; Louis, J.; Debaecker, V.; Müller-Wilm, U.; Gascon, F. Sen2Cor for Sentinel-2. In *Image and Signal Processing for Remote Sensing XXIII*; Bruzzone, L., Bovolo, F., Benediktsson, J. A., Eds.; SPIE, 2017; p. 3.

32. De Keukelaere, L.; Sterckx, S.; Adriaensen, S.; Knaeps, E.; Reusen, I.; Giardino, C.; Bresciani, M.; Hunter, P.; Neil, C.; Van der Zande, D.; Vaiciute, D. Atmospheric correction of Landsat-8/OLI and Sentinel-2/MSI data using iCOR algorithm: validation for coastal and inland waters. *Eur. J. Remote Sens.* **2018**, *51*, 525–542, doi:10.1080/22797254.2018.1457937.

33. Swets, D. L.; Reed, B. C.; Rowland, J. R.; Marko, S. E. A weighted least-squares approach to temporal smoothing of NDVI. In *1999 ASPRS Annual Conference, From Image to Information*; 1999.

34. Breiman, L. Random Forests. *Mach. Learn.* **2001**, *45*, 5–32, doi:10.1023/A:1010933404324.

35. Belgiu, M.; Drăguţ, L. Random forest in remote sensing: A review of applications and future directions. *ISPRS J. Photogramm. Remote Sens.* **2016**, *114*, 24–31, doi:10.1016/j.isprsjprs.2016.01.011.

36. Bostrom, H. Estimating class probabilities in random forests. In *Sixth International Conference on Machine Learning and Applications (ICMLA 2007)*; IEEE, 2007; pp. 211–216.

37. Belgiu, M.; Csillik, O. Sentinel-2 cropland mapping using pixel-based and object-based time-weighted dynamic time warping analysis. *Remote Sens. Environ.* **2018**, *204*, 509–523, doi:10.1016/j.rse.2017.10.005.

38. Xiong, J.; Thenkabail, P.; Tilton, J.; Gumma, M.; Teluguntla, P.; Oliphant, A.; Congalton, R.; Yadav, K.; Gorelick, N. Nominal 30-m Cropland Extent Map of Continental Africa by Integrating Pixel-Based and Object-Based Algorithms Using Sentinel-2 and Landsat-8 Data on Google Earth Engine. *Remote Sens.* **2017**, *9*, 1065, doi:10.3390/rs9101065.

39. Veloso, A.; Mermoz, S.; Bouvet, A.; Le Toan, T.; Planells, M.; Dejoux, J.-F.; Ceschia, E. Understanding the temporal behavior of crops using Sentinel-1 and Sentinel-2-like data for agricultural applications. **2017**, doi:10.1016/j.rse.2017.07.015.

40. Pereira, L. de O.; Freitas, C. da C.; Sant´Anna, S. J. S.; Lu, D.; Moran, E. F. Optical and radar data integration for land use and land cover mapping in the Brazilian Amazon. *GIScience Remote Sens.* **2013**, *50*, 301–321, doi:10.1080/15481603.2013.805589.

41. Erasmi, S.; Twele, A. Regional land cover mapping in the humid tropics using combined optical and SAR satellite data—a case study from Central Sulawesi, Indonesia. *Int. J. Remote Sens.* **2009**, *30*, 2465–2478, doi:10.1080/01431160802552728.

42. Chureesampant, K.; Susaki, J. Land Cover Classification Using Multi-Temporal Sar Data and Optical Data Fusion With Adaptive Training Sample. *Ieee/ Igarss* **2012**, 6177–6180, doi:10.1109/IGARSS.2012.6352667.

43. Campos-Taberner, M.; García-Haro, F.; Camps-Valls, G.; Grau-Muedra, G.; Nutini, F.; Busetto, L.; Katsantonis, D.; Stavrakoudis, D.; Minakou, C.; Gatti, L.; Barbieri, M.; Holecz, F.; Stroppiana, D.; Boschetti, M. Exploitation of SAR and Optical Sentinel Data to Detect Rice Crop and Estimate Seasonal Dynamics of Leaf Area Index. *Remote Sens.* **2017**, *9*, 248, doi:10.3390/rs9030248.

44. Inglada, J.; Vincent, A.; Arias, M.; Marais-Sicre, C. Improved Early Crop Type Identification By Joint Use of High Temporal Resolution SAR And Optical Image Time Series. *Remote Sens.* **2016**, *8*, 362, doi:10.3390/rs8050362.

45. Castillejo-González, I. L.; López-Granados, F.; García-Ferrer, A.; Peña-Barragán, J. M.; Jurado-Expósito, M.; de la Orden, M. S.; González-Audicana, M. Object- and pixel-based analysis for mapping crops and their agro-environmental associated measures using QuickBird imagery. *Comput. Electron. Agric.* **2009**, *68*, 207–215, doi:10.1016/j.compag.2009.06.004.